Ocean Dynamics (2020) 70:603–619
https://doi.org/10.1007/s10236-020-01350-y

Oceanic response to Hurricane Irma (2017) in the Exclusive Economic Zone of Cuba and the eastern Gulf of Mexico

Dailé Avila-Alonso[1,2] · Jan M. Baetens[2] · Rolando Cardenas[1] · Bernard De Baets[2]

Received: 21 October 2019 / Accepted: 27 January 2020 / Published online: 5 March 2020

Abstract

An understanding of the oceanic response to tropical cyclones is of importance for studies on climate change, ecological variability and environmental protection. Hurricane Irma (2017, Atlantic Ocean) broke many records, including the fact that it was the first category 5 hurricane making landfall in Cuba since 1924. In this study, we assess the oceanic response of the waters of the Cuban Exclusive Economic Zone (EEZ) and the eastern Gulf of Mexico (GoM) to the passage of this hurricane. Overall, Irma led to a weak sea surface cooling in the EEZ, which was associated with the thermal structure of its waters and the fact that it was affected by the left-side quadrants of this hurricane. This cooling was driven by mixing and upwelling processes. In contrast, the chlorophyll-a (chl-a) concentration increase was comparable with climatological records, suggesting that horizontal advection of coastal waters and entrainment of chl-a rich waters from remote regions of the GoM influenced the post-storm chl-a concentration. Moreover, Irma increased the chl-a concentration in the northeastern GoM and stimulated the offshore transport of these chl-a-rich waters to the interior GoM. A high chl-a plume (HCP) extended southward across the eastern GoM during the first post-storm week of Irma, and these waters reached the northwestern Cuban coast following the Loop Current. An intensification of the geostrophic currents of an anticyclonic eddy at the upper front of the Loop Current, the formation of an anticyclonic-cyclonic eddy pair in the northeastern GoM and wind-driven advection governed the extension of this HCP.

Keywords Chlorophyll-a concentration · Exclusive Economic Zone of Cuba · Hurricane Irma · Remote sensing · Sea surface temperature

1 Introduction

Tropical cyclones (TCs) are extreme environmental phenomena having substantial effects on the upper oceanographic conditions (Price 1981). Oceanic response to TCs has been a hot topic given its importance for studies on climate change, ecological variability and environmental protection (Fu et al. 2014). Over oceans, TC-induced wind forcing mixes the surface layer, deepens the mixed layer and induces a decrease in sea surface temperature (SST) (Price 1981; Shay and Elsberry 1987). Vertical mixing and upwelling lead to an increased abundance of surface phytoplankton via two vertical transport pathways, i.e. entrainment of nutrient-rich waters from the nitracline to the ocean surface and/or entrainment of phytoplankton from the deep chlorophyll maximum (Babin et al. 2004; Walker et al. 2005a; Gierach and Subrahmanyam 2008; Shropshire et al. 2016). The nutrient influx coupled with adequate sunlight stimulates phytoplankton growth and can lead to phytoplankton blooms lasting several days after the TC passage in very oligotrophic oceanic waters (Babin et al. 2004; Hanshaw et al. 2008; Shropshire et al. 2016).

On the other hand, as a TC makes landfall, the coastal land is inundated with convective rain and storm surge. This heavy rainfall leads to a substantial input of nutrients and organic matter through freshwater river discharges that can also trigger phytoplankton blooms in coastal waters (Mallin et al. 1993; Farfán et al. 2014; Anglès et al. 2015). Moreover, interaction of TCs with coastal waters can lead to the advection of these highly productive coastal waters to the open ocean (Acker et al. 2009). Thus, both vertical and horizontal transport pathways can modulate the biological response following a TC (Avila-Alonso et al. 2019).

Responsible Editor: Christoph Voelker

✉ Dailé Avila-Alonso
davila@uclv.cu

1 Laboratory of Planetary Science, Department of Physics, Universidad Central “Marta Abreu” de Las Villas, 54830 Santa Clara, Villa Clara, Cuba

2 KERMIT, Department of Data Analysis and Mathematical Modelling, Faculty of Bioscience Engineering, Ghent University, 9000 Ghent, Belgium

A combination of in situ and remotely sensed measurements enables the best characterization of ocean waters (Meyers et al. 2016). Some authors have used both types of observation to assess the oceanic post-storm response (e.g. Fuentes Yaco et al. 2007; Meyers et al. 2016; Wang et al. 2016). However, given the limitations induced by weather conditions on in situ measurements during the passage of TCs, satellite data are promising sources of information to further our understanding of the TC-induced oceanographic variability (Son et al. 2007). Hence, several studies have assessed the oceanic response to TCs on the basis of satellite data in the North Atlantic Basin in general (e.g. Babin et al. 2004; Hanshaw et al. 2008; Foltz et al. 2015; Shropshire et al. 2016) and the Gulf of Mexico (GoM) and the Caribbean Sea in particular (e.g. Gilbes et al. 2001; Gilbes and Armstrong 2004; Walker et al. 2005a; Gierach and Subrahmanyam 2008; Shi and Wang 2007; Acker et al. 2009; Pérez-Santos et al. 2014; Avila-Alonso et al. 2019). From satellite imagery, an increase in phytoplankton abundance is identified as elevated chlorophyll-a (chl-a) concentration. Distinguishing between mechanisms inducing this change is crucial to understanding the impact of storms on surface oceanographic conditions.

The Atlantic Hurricane Season in 2017 showed an activity well above the normal (Trenberth et al. 2018). In particular, Hurricane Irma broke many records including the longest lifetime as a category 5 storm on the Saffir-Simpson hurricane scale. Besides, it was the first category 5 hurricane making landfall in Cuba since 1924 and it produced the most accumulated cyclone energy of any storm in the tropical Atlantic ever (Trenberth et al. 2018). Given that Irma made landfall in Cuba and the Florida Peninsula, it may be thought that the induced oceanic response in this region could have been influenced by coastal processes.

The long-term oceanic response of the waters of the Exclusive Economic Zone (EEZ) of Cuba to the passage of hurricanes in the period 1998–2016 has recently been assessed (Avila-Alonso et al. 2019). Marine research in the EEZ meets the need to manage sea exploitation and conservation at the national level according to the Marine Spatial Planning Programme of the UNESCO Intergovernmental Oceanographic Commission (Meaden et al. 2016). Countries must manage fisheries within their EEZs (Prescott-Allen 2001). Since fisheries are ultimately linked to the patterns of phytoplankton production, an assessment of the oceanographic variability under normal and extreme meteorological conditions is crucial to comprehending the possible effects on fisheries resources. The waters surrounding Cuba are pelagic larval nursery areas for the spiny lobster *Panulirus argus* (Latreille, 1804) (Kough et al. 2013). These are areas in the open Caribbean Sea where lobster larvae from the Caribbean spend much of their planktonic existence before settling in coastal benthic nurseries (Kough et al. 2013). Given that the TC-induced oceanographic variability can lead to fluctuations of *P. argus* recruitment in the GoM and the Caribbean Sea (Briones-Fourzán et al. 2008), an assessment of the oceanic response to TCs serves for future studies on fishery oceanography in the region. However, the possible oceanic effects induced by Irma in the waters of the EEZ of Cuba have not yet been studied.

In this work, we assess the oceanic response of the waters of the EEZ of Cuba and the eastern GoM to the passage of Irma using remotely sensed data as primary source of information, thus extending the study of Avila-Alonso et al. (2019). The latter region was included in our analysis because the storm-induced oceanographic variability in it impacted the oceanic response of the EEZ of Cuba. The methods adopted and the considered data sets are introduced in Sect. 2. Next, in Sect. 3, we present the synoptic history of Irma and the oceanic changes it induced, followed by a discussion of the observed storm-induced variability (Sect. 4).

2 Materials and methods

2.1 Methodology

The oceanic response to TCs has been assessed in ocean parcels along the TC trajectory (Babin et al. 2004; Menkes et al. 2016; Shropshire et al. 2016). Yet, using this approach to evaluate the oceanic response induced by Irma in the waters surrounding Cuba is difficult because Irma passed across the narrowest area of the EEZ of Cuba (Fig. 1). Besides, north of the northern EEZ of Cuba lies the Great Bahama Bank (GBB), which has oligotrophic and shallow waters (3 to 10 m) (Dierssen et al. 2010). The GBB is, for the most part, optically shallow, in that reflectance of the seafloor contributes to the reflected light measured by satellites (Dierssen et al. 2010), which leads to data quality issues when quantifying, for instance, chl-a (Boss and Zaneveld 2003). Overall, although Irma mainly moved over oceanic waters of the Old Bahamas Channel, its trajectory was surrounded by shallow and coastal waters of Cuba and The Bahamas. In order to quantify the oceanic response along the trajectory of Irma, we studied the part of the EEZ directly affected by the centre of this hurricane (Fig. 1). We refer to this area as the along-track sector, which has a mean depth of approximately 1000 m according to the ETOPO1 model.

Although Irma moved across the northern waters of Cuba, its outer spiral rain bands extended over the entire EEZ (see Fig. 6 in the Irma TC report of the National Hurricane Center (NHC), https://www.nhc.noaa.gov/data/tcr/AL112017_Irma.pdf). For that reason, we also assessed the oceanic response throughout the entire EEZ. Given that the hurricane-induced oceanographic variability is associated with the pre-storm conditions of the ocean (Menkes et al.

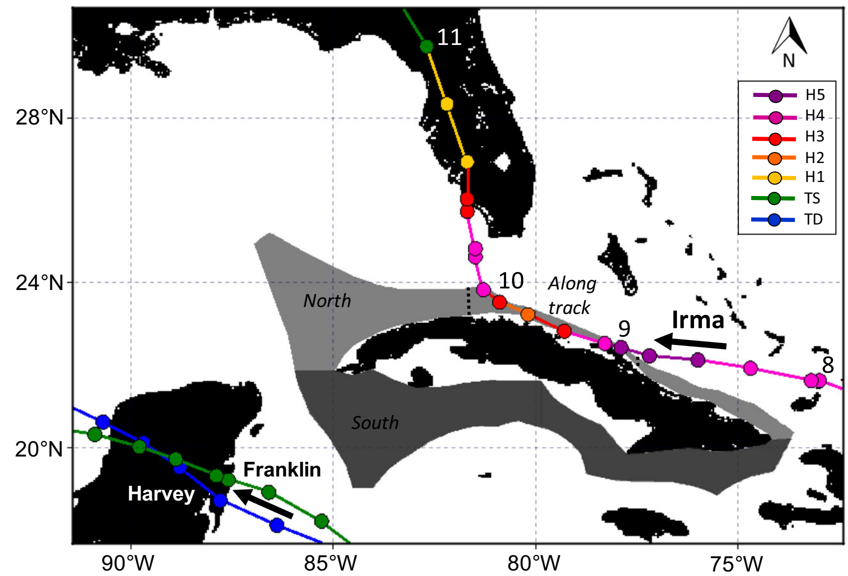

Fig. 1 Trajectory of tropical cyclones (TCs) Irma, Harvey and Franklin (2017). Colours indicate the TC category (i.e. TD: Tropical depression, TS: Tropical storm, H1–H5: Saffir Simpson Hurricane Categories). Numbers along the trajectory of Irma indicate the day. The Exclusive Economic Zone (EEZ) of Cuba is represented by the grey area surrounding Cuba, where light and dark grey represent the northern and southern sectors, respectively. The along-track sector in the EEZ is indicated by the dotted lines. The forward direction of the TCs is indicated by arrows

2016) and considering that the northern and southern waters of Cuba have different oceanographic conditions, i.e. the southern waters are warmer and less productive that the northern ones (González et al. 2000; Cerdeira-Estrada et al. 2005), we assessed the oceanic response in the northern and southern sectors of the EEZ separately (Fig. 1). These have a mean depth of 2024 and 3697 m, respectively, according to the ETOPO1 model.

The oceanic response to the passage of a TC can be divided into two stages, i.e. the forced stage (when the TC is overhead the study area) and the relaxation stage (after the TC leaves the study area) (Jaimes and Shay 2015). We assessed the daily response of the oceanographic variables before, during and after the passage of Irma. We considered the pre-storm week (i.e. days −10 to −3 before hurricane passage) as a benchmark for comparison with the post-storm weeks in agreement with the procedure followed by Vincent et al. (2012) and Menkes et al. (2016). It has been reported that the storm-induced SST cooling can last up to a month after the TC passage (Menkes et al. 2016; Avila-Alonso et al. 2019). However, in the fourth post-storm week of Irma, the tropical storm Nate passed between the Yucatan Peninsula and the northwestern tip of Cuba leading to clouds during its pre- and post-storm weeks. Thus, we limited our study to 2 weeks after the entrance of Irma in the EEZ (i.e. from day 0 to + 15, where day 0 refers to the day the hurricane entered the study area) (Vincent et al. 2012; Menkes et al. 2016; Avila-Alonso et al. 2019). Besides, the oceanic response of the eastern GoM was analysed for the mentioned pre- and post-storm weeks considering the day that Irma entered the EEZ as reference.

Daily and weekly arithmetic means were computed for each analysed variable. We calculated the mean daily value of the pixel data within each sector of the EEZ. Because of cloud-induced gaps and incomplete spatial coverage as a consequence of satellite orbits, we only analysed mean daily data for images with more than 50% of pixel data in the sectors of the EEZ. Weekly means were then calculated from these daily means. We also computed standardized anomalies by subtracting the mean pre-storm week value from the daily values (from day − 10 to day + 15), in agreement with the procedure followed by Menkes et al. (2016). We calculated the translation speed of Irma when it had hurricane strength in general, and within the EEZ of Cuba and in the eastern GoM (i.e. from the EEZ to the last point of its trajectory as hurricane) in particular. For this purpose, we followed the procedure outlined by Babin et al. (2004) and Gierach and Subrahmanyam (2008).

2.2 Data

The shapefile of the EEZ of Cuba was obtained from the world EEZ product (version 9) (http://www.marineregions.org/downloads.php) of the Flanders Marine Institute, where the inner boundary of the EEZ is used as a proxy for the low water line. We obtained the hurricane trajectory from the International Best Track Archive for Climate Stewardship (IBTrACS v03r03) (Knapp et al. 2010) (ftp://eclipse.ncdc.noaa.gov/pub/ibtracs/v03r09/all/shp). Besides, the reported "best track" observations of time and position from the hurricane database (HURDAT2) of the NHC (http://www.aoml.noaa.gov/hrd/hurdat/hurdat2.html) were used to calculate the translation speed.

2.2.1 Response variables

We considered SST and chl-a concentration as the main physical and biological oceanographic response variables, respectively. SST data were derived from the Operational SST and Sea Ice Analysis (OSTIA) Near Real Time Level 4 product (Donlon et al. 2012) provided by the Copernicus Marine Environment Monitoring Service (http://marine.copernicus.eu). OSTIA merges both infrared and microwave radiometer data, together with in situ observations at a spatial resolution of 0.05° × 0.05°. The chl-a images were obtained from the multisatellite merged global data of the GlobColour project (http://globcolour.info), developed, validated and distributed by ACRI-ST, France. We used the chl-a concentration data computed with the OC5 algorithm at a spatial resolution of 0.0417° × 0.0417°. This method is empirical and derived from the OC4/Sea-Viewing Wide Field-of-View Sensor (SeaWiFS) algorithm of NASA (or OC3M-547 for Moderate Resolution Imaging Spectroradiometer (MODIS) and OC4E for Medium Resolution Imaging Spectrometer (MERIS)) (Gohin 2011). It uses the 412 and 555 nm wavelengths accounting for the effects of coloured dissolved organic matter (CDOM) and suspended matter, respectively (Gohin et al. 2002; Gohin 2011).

In general, the deep waters surrounding Cuba are considered as Case 1 waters (Matsushita et al. 2012; Mélin and Vantrepotte 2015), according to the classification of Morel (1980). Hence, chl-a (and its associated degradation products) is a major factor affecting its optical properties (Mélin and Vantrepotte 2015). However, after a TC passage, marine waters become Case 2 of the Morel (1980) classification (i.e. waters with high concentrations of CDOM and total suspended matter) since, for instance, the storm-induced mixing and upwelling can transport deep oceanic waters containing CDOM to the surface (Acker et al. 2009). Moreover, given that Irma crossed close to the Cuban coast, horizontal advection of optically complex coastal waters is expected. In this sense, the OC5 algorithm is suitable for assessing storm-induced chl-a response given its potential to quantify chl-a concentration across a large range of optically complex waters (Loisel et al. 2017).

Although SST has been widely used to assess storm-induced cooling, it only gives insight into the sea surface variability. This limitation can be avoided by using the upper ocean heat content (OHC), which is the integrated vertical temperature from the sea surface to the 26 °C isotherm depth (Leipper and Volgenau 1972; Price 2009). We used daily OHC data from the Systematically Merged Regional Atlantic Temperature and Salinity (SMARTS) Climatology adjusted to a two-layer reduced gravity model at a spatial resolution of 0.25° × 0.25° (Meyers et al. 2014). Meyers et al. (2016) found that OHC estimates were fairly accurate in the GoM for assessments to the passage of Hurricane Gustav (2008). All SMART Climatology data were provided by the Upper Ocean Dynamics Laboratory at the University of Miami Rosenstiel School of Marine and Atmospheric Sciences (www.rsmas.miami.edu/groups/upper-ocean-dynamics).

2.2.2 Drivers of ocean cooling

The TC-induced oceanic cooling results from the combined effects of heat loss to the storm across the air-sea interface, upwelling of cooler thermocline waters (Ekman pumping), and turbulent vertical entrainment of cooler thermocline waters across the ocean mixed layer (Price 1981; Jaimes and Shay 2015). These processes are strongly related to TC winds (Wei et al. 2018, and references therein) and other factors (e.g. Sun et al. 2010; Sun et al. 2014). It has been suggested that those wind-driven processes govern the post-storm SST cooling in the waters of the Cuban EEZ due to the high and statistically significant correlation of wind speed and SST (Avila-Alonso et al. 2019). Several studies have documented the occurrence of upwelling and vertical mixing in the waters surrounding Cuba after the passage of hurricanes (e.g. Oey et al. 2006; Oey et al. 2007; Meyers et al. 2016), but the main physical processes underlying the upper-ocean cooling across the entire EEZ of Cuba during and after the passage of hurricanes are not yet understood. For that reason, we assessed the variability of the mixed layer and the thermocline displacement during the forced and relaxation stages of Irma in the EEZ of Cuba, as well as the temporal evolution of wind speed as the potential main driver of such responses. We used the Cross-Calibrated Multi-Platform (version 2.0) 6-hourly gridded ocean vector wind (to a height of 10 m) data (Atlas et al. 2011) at a spatial resolution of 0.25° × 0.25° produced by Remote Sensing Systems (data available at ftp://ftp.remss.com/ccmp/v02.0). We determined the daily wind speed by averaging the 6-hourly products.

Upwelling and downwelling regimes can be identified by analysing the fluctuations in the 20 °C isotherm depth (D20) in the GoM because wind-driven vertical mixing is confined to waters above this depth (Price 1983; Jaimes and Shay 2009; Jaimes and Shay 2015). Thus, D20 has been considered as a proxy of the thermocline in the GoM (Jaimes and Shay 2009; Jaimes and Shay 2015) where it was reported to be about 200–250 m in the Loop Current and 100–120 m in cold-core eddies (Jaimes and Shay 2009). We quantified the upwelling responses in terms of fluctuations in D20, by computing the difference between pre- and post-storm D20 values as in Meyers et al. (2016). We inferred daily D20 from the SMARTS Climatology.

Given that the MLD is not directly measurable, extensive data sets are lacking (both in situ and satellite-sensed data). The SMARTS Climatology provides an MLD product, but even though these MLD data seem to be consistent with in situ observations for the GoM (including the NWS of the EEZ of Cuba) under normal meteorological conditions, they do not capture the extensive deepening of the mixed layer after the passage of hurricanes (Meyers et al. 2016). Thus, we derived daily data of MLD from the vertical profiles of temperature produced by the Global Ocean Physics Analysis and Forecast model MERCATOR PSY 4QV3R1. We considered the Levitus criterion (Levitus 1982) to define the surface isothermic layer, i.e. the bottom of the mixed layer is defined as the depth where temperature is 0.5 °C lower than the surface temperature, as in previous studies in the waters surrounding Cuba (Mitrani Arenal 2001; Mitrani Arenal and Rodríguez 2001).

2.2.3 High chlorophyll plume

As we will show in Sect. 3, a high chl-a plume (HCP) extending from the northeastern GoM to the central basin was observed during the pre- and the post-storm weeks of Irma. Given that these chl-a-rich waters reached the northwestern EEZ of Cuba after the passage of Irma and consequently impacted the chl-a concentration in the region, we aim at identifying the origin of this HCP as well as the main mechanisms driving it. Commonly, HCPs have a high concentration of CDOM and non-algal particles (NAP, i.e. detrital organic and inorganic particulates). Because of the strong relationship between CDOM and dissolved organic carbon (DOC) (Spencer et al. 2013), the former can be used as a tracer of terrigenous DOC (Zhu et al. 2011), while DOC has been used as a tracer of river plumes (da Silva and Castelao 2018). Given the similar absorption spectra of CDOM and NAP, they are often combined together as a single optical product, i.e. as a coloured dissolved and detrital organic material absorption coefficient (CDM) (Matsuoka et al. 2013 and references therein). However, CDOM and NAP have a different dynamics in the ocean since, for instance, particles sink rather quickly at a vertical speed ranging from a few meters to several hundred meters per day (Fischer and Karakaş 2009), while CDOM can be transported by ocean currents over long distances (Matsuoka et al. 2011; Matsuoka et al. 2012). Consequently, we analysed CDM at 443 nm to corroborate the riverine origin of the observed HCP. They were obtained from the GlobColour project computed with the Garver, Siegel and Maritorena model (0.0417° × 0.0417° of spatial resolution) (Maritorena et al. 2010).

Given that in river plumes up to 50% of the remotely sensed chl-a concentration could be an artefact of the high CDOM concentration (Hochman et al. 1994), we also analysed the phytoplankton absorption coefficient at 443 nm (a_{ph}) provided by MODIS Aqua (https://oceancolor.gsfc.nasa.gov) at a spatial resolution of 0.0417° × 0.0417°. This enabled us to confirm that the chl-a increase in the HCP was related to the presence of phytoplankton. On the other hand, HCPs can also be tracked as filaments of low-salinity waters which primarily originate from river discharge in coastal zones (Morey et al. 2003a; da Silva and Castelao 2018). Thus, we also analysed sea surface salinity (SSS) data to draw sound conclusions on the riverine origin of the HCP. More specifically, we used daily SSS data derived from the Operational Mercator Global Ocean Analysis and Forecasting System at a spatial resolution of 0.083° × 0.083° (http://marine.copernicus.eu). The Global Analysis and Forecasting System PSY4V3R1 uses version 3.1 of the NEMO ocean model (Madec 2008).

On the other hand, considering that both wind- and eddy-driven dynamics play major roles in the transport and dispersion of HCPs in the GoM (Walker et al. 2005a; Schiller et al. 2011; Jones and Wiggert 2015), we analysed wind speed, geostrophic current sand sea surface height anomaly (SSHA) data to identify the environmental drivers governing the horizontal advection of chl-a-rich waters to the central GoM. We used daily satellite wind speed data derived from the Cross-Calibrated Multi-Platform (version 2.0) (Atlas et al. 2011). Besides, we used the Salto/DUACS gridded multimission altimeter data of SSHA and the zonal and meridional components of the absolute geostrophic currents. These data have a spatial resolution of 0.25° × 0.25°, and are processed and distributed by the Copernicus Marine Environment Monitoring Service.

3 Results

3.1 Synoptic history and classification of Hurricane Irma

According to the TC report of the NHC (https://www.nhc.noaa.gov/data/tcr/AL112017_Irma.pdf), Irma originated from a tropical wave that departed from the west coast of Africa on 27 August 2017 and intensified rapidly while moving westward, and finally reached the hurricane category on 31 August. Irma made its first landfall on Barbuda island on 6 September as a category 5 hurricane and continued moving west-northwestward across the Caribbean entering the EEZ of Cuba on 9 September as a category 5 hurricane (Fig. 1), where it weakened to a category 2. Then, early on 10 September Irma turned to the northwest, and moved over the warm waters of the Florida Strait where it reintensified to major hurricane (i.e. higher than category 3) and made final landfall near Marco Island, Florida, at that day (Fig. 1). Once inland over southwestern Florida, Irma weakened quickly and became a TC of lower intensity on 11 September, though its tropical-storm-force winds extended up to 667 km from the centre. After that, Irma continued across northern Florida, southern Georgia and became a remnant low over Alabama on 12 September. Finally, it dissipated shortly after on 13 September over southeastern Missouri.

TCs are classified into two groups either by their maximum sustained wind speed (strong or weak TCs) or by their translation speed (fast or slow moving TCs) (Fu et al. 2014). According to its maximum sustained wind speed, Irma was a strong TC considering the criterion of Fu et al. (2014) (i.e.

> 33 m s^{-1}). Overall, the mean maximum sustained wind speed across the Cuban EEZ was 60 m s^{-1}, while this was 49 m s^{-1} over the Florida Strait and the Florida Peninsula (until the last track point where it had hurricane strength) according to HURDAT2 data. Several thresholds have been used to classify TCs on the basis of their translation speed (Bender et al. 1993; Lonfat et al. 2004; Fu et al. 2014; Domingues et al. 2015). Given this variability and considering that classification of TCs on the basis of their translation speed is very latitude dependent, we compared the computed translation speed of Irma with the climatological records of Atlantic hurricanes derived from the HURDAT2 data (see table in http://www.aoml.noaa.gov/hrd/tcfaq/G16.html). So, we considered that a fast (slow) moving TC has a higher (lower) translation speed than the climatological one for the concerned latitudinal band.

The entire trajectory of Irma was largely restricted to the latitudinal band 15–30°N (see Fig. 1 in Irma TC Report), for which the mean climatological translation speed of Atlantic hurricanes is 18.3 km h^{-1}. Irma had a mean translation speed of 20.41 km h^{-1} (5.67 m s^{-1}), so, it may be considered as a fast moving hurricane. Moreover, across the Cuban EEZ, Irma moved at 17.04 km h^{-1} (4.73 m s^{-1}), while the climatological translation speed in the latitudinal band 20–25°N (that of the Cuban EEZ) is 17.4 km h^{-1}. So, Irma can be considered as a moderately fast-moving hurricane in this region, and this slight slowdown was related to the turn Irma made to the northwest in the direction of the Florida Strait (Fig. 1). Then, over the Florida Strait and the Florida Peninsula (until the last track point where it had hurricane strength), Irma advanced at a mean translation speed of 21.27 km h^{-1} (5.91 m s^{-1}), which is higher than the climatological translation speed in the latitudinal band 25–30°N (i.e. 20.1 km h^{-1}). All together, it can be concluded that Irma was a strong and fast-moving TC.

3.2 Oceanic response in the waters of the Exclusive Economic Zone of Cuba

3.2.1 Sea surface temperature and ocean heat content

During the pre-storm week of Irma, the highest SST values were observed south of Cuba, around The Bahamas and along the West Florida Shelf. On the other hand, the lowest SST values were observed north of the Yucatan Peninsula (Fig. 2a). The latter could be related to the coastal upwelling system of the Campeche Bank (Zavala-Hidalgo et al. 2006) and to the passage of TCs Franklin and Harvey across the Yucatan Peninsula in August (Fig. 1), which led to a SST decrease of 0.9 and 0.1 °C during their first post-storm week, respectively. After the passage of Irma across the northern waters of Cuba, a sea surface cooling occurred over the entire EEZ during the first post-storm week, although it was the most substantial in the northern sector and along Irma trajectory (Fig. 2b, c). In contrast, a considerable decrease of the OHC was only observed along the trajectory (Fig. 2d). Specifically, Irma induced a weak SST (and OHC) decrease since mean SST during the first post-storm week only dropped 0.7, 1.4 and 1.6% in the north, south and along-track sectors, respectively. Along the trajectory, 93 and 97% of SST anomalies accounted for surface cooling of less than 1 °C during the first and second post-storm weeks, respectively. Moreover, Irma led to a significant weaker SST cooling (Mann-Whitney test, $p < 0.05$) both along the trajectory (− 0.49 °C) and over the entire EEZ (− 0.1 °C) as compared with climatological records (i.e. − 0.63 °C along the trajectory and − 0.47 °C over the entire EEZ) during the first two post-storm weeks (Avila-Alonso et al. 2019).

Drivers of the post-storm cooling The surface wind speed anomalies in the Cuban EEZ had a distinct dynamics during the passing of a hurricane (Fig. 3a). In general, wind speed values where higher along track since the spatially averaged data at this scale account for the eyewall winds (Fig. 3a). However, spatially averaged winds across the northern and southern sectors as a whole had similar values given the vast extent of the strong winds of Irma. Hurricane winds can generate inertial currents in the upper ocean (Gonella 1971), as such leading to mixing of the upper oceanic layer (Prakash et al. 2018). We found fluctuations of the MLD during and immediately after the passage of Irma across the EEZ of Cuba. In general, Irma led to a maximum deepening of the mixed layer of 15 and 8 m in the northern and southern sectors, respectively, and 25 m along track (Fig. 3b). Then, after this maximum deepening, a sudden shoaling of the MLD was observed around days 4–6 (Fig. 3b), which is consistent with the increased number of pixels indicating post-storm upwelling (Fig. 3c) and the most pronounced upward displacement of the thermocline (Fig. 3d). This largely agrees with the findings of Wu and Chen (2012) for the North Pacific Ocean, who reported that, on average, the mixed layer returns to its pre-storm depth about 5 days after the passage of a TC.

It has been reported that upwelling can reduce the MLD, increase entrainment efficiency at the mixed layer base and bring more cold water to cool the surface mixed layer (Sun et al. 2012; Zhang et al. 2016). Hence, the strongest cooling of surface and subsurface waters was observed during the relaxation stage (Fig. 2c, d) and was driven by upwelling of the thermocline. Overall, entrainment has been considered the dominant process leading to ocean surface cooling after the passage of TCs due to the mixing of the surface waters with upwelled cold waters (Price 1981; D'Asaro et al. 2007; Jullien et al. 2012). On the other hand, the rise of OHC during the forced stage in all sectors of the EEZ can be associated with extensive downwelling events at this time (Fig. 3c), which led to a subsurface warming (Jaimes and Shay 2015; Zhang et al.

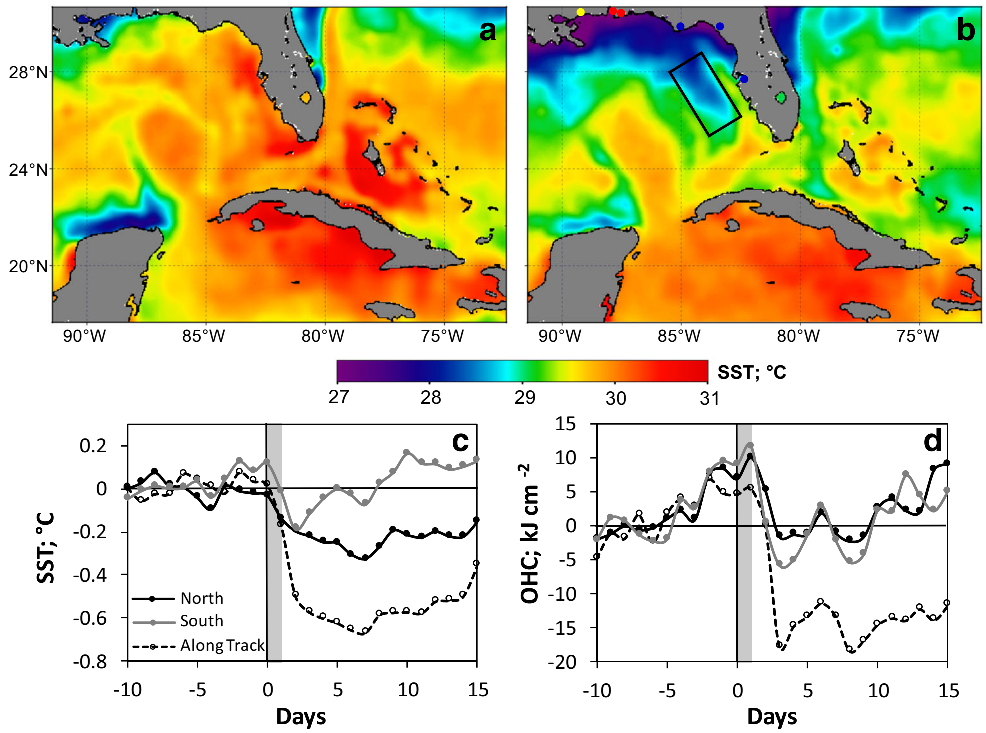

Fig. 2 Weekly mean sea surface temperature (SST) values in the (**a**) pre- and (**b**) first post-storm week of Irma. The coloured circles in (**b**) indicate the stations along the northeast coast of the Gulf of Mexico (GoM) where river discharge was measured in Florida (blue circles), Alabama (red circles) and Mississippi (yellow circle). The rectangle in (**b**) indicates the tongue of cool waters in the northeastern GoM. Daily mean evolution of anomalies of (**c**) SST and (**d**) ocean heat content (OHC) in the Exclusive Economic Zone of Cuba (EEZ) of Cuba before and after the passage of Irma. The grey bands in (**c**) and (**d**) indicate the forced stage of Irma in the EEZ of Cuba

2019). TCs typically produce an energetic upwelling flow underneath the storm centre and weak downwelling of the displaced warm water over a broad area outside upwelled regions (Price 1981; Jullien et al. 2012; Fu et al. 2014; Liu et al. 2017). Given that only a small area of the EEZ of Cuba was affected by the storm centre as compared with that exposed to its outer spiral bands, spatially averaged data of OHC essentially captured the latter response.

3.2.2 Chlorophyll-a concentration

For what concerns the oceanic biological response to the passage of Irma, we found that the chl-a concentration increased over the entire EEZ of Cuba during the first and the second post-storm weeks, although it was the most pronounced in the northern sector and along Irma's track (Fig. 4b, d). Specifically, chl-a concentration increased by

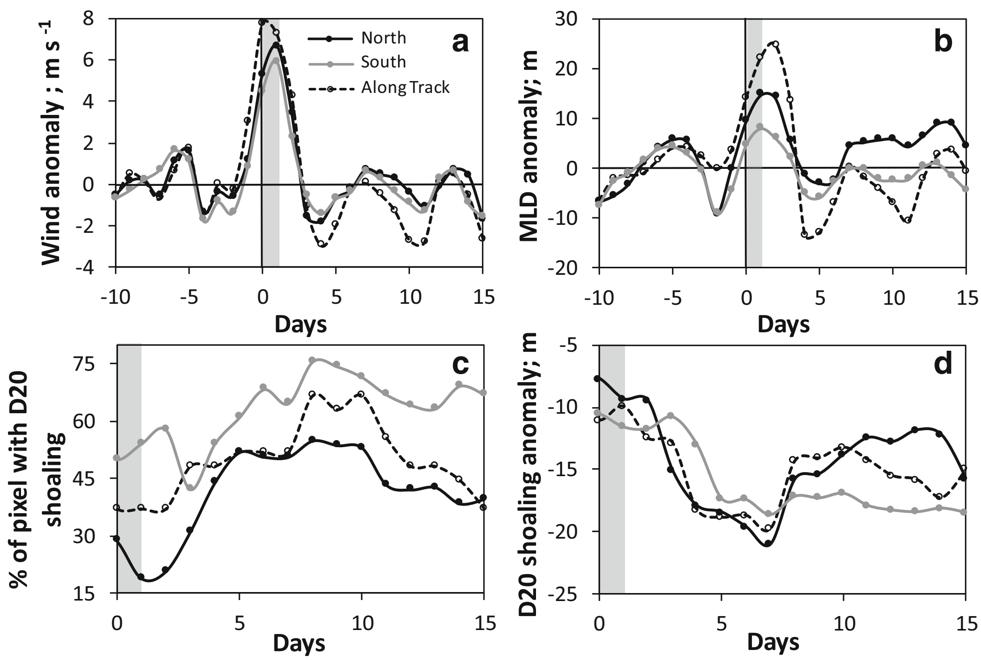

Fig. 3 Daily mean evolution of anomalies of (**a**) wind speed and (**b**) mixed layer depth (MLD) in the Exclusive Economic Zone (EEZ) of Cuba before and after the passage of Irma. (**c**) Percentage of pixels within each sector indicating upwelling after the passage of Irma. From those pixels with upwelling, (**d**) displays the magnitude of the upward displacement of 20 °C isotherm depth (D20) as a measure of the thermocline upwelling. The grey bands indicate the forced stage of Irma in the EEZ of Cuba

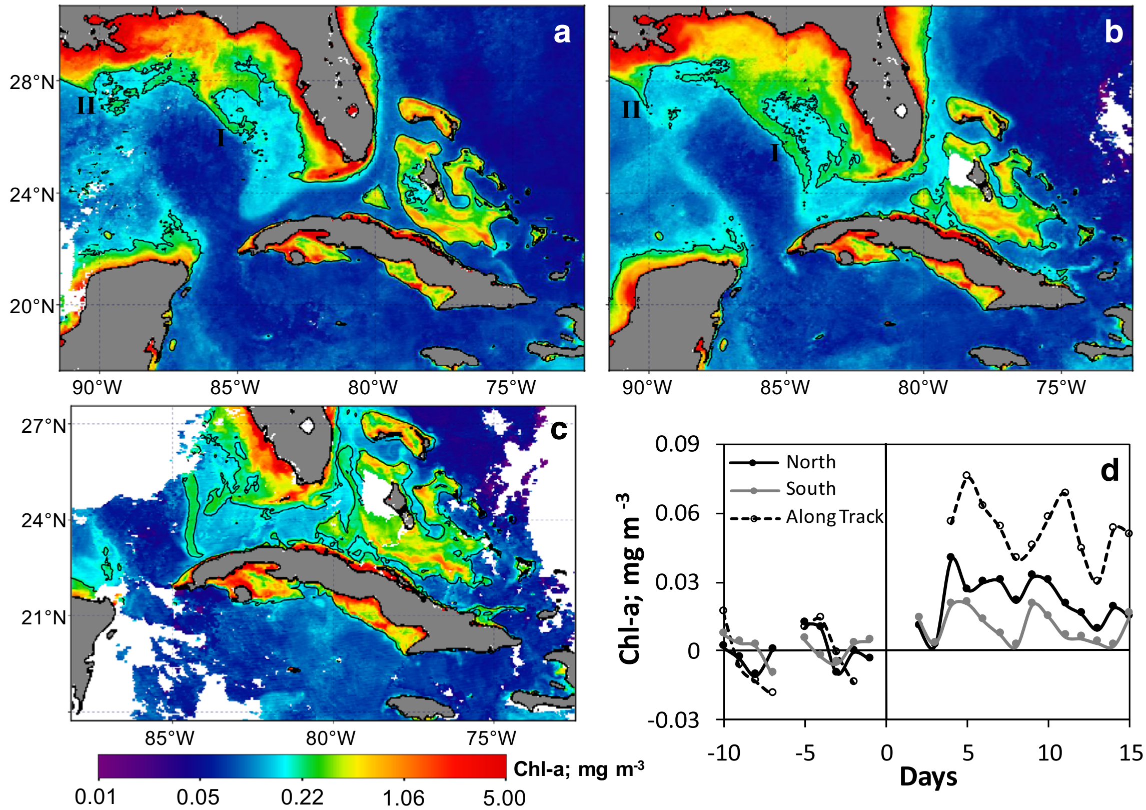

Fig. 4 Weekly mean chlorophyll-a (chl-a) concentration in the (**a**) pre- and (**b**) first post-storm week of Irma. (**c**) Chl-a increase on 14 September. The contour lines delineate chl-a concentration values 0.2 mg m^{-3} apart. The white pixels are due to clouds. (**d**) Daily mean evolution of the chl-a concentration anomalies in the Exclusive Economic Zone of Cuba before and after the passage of Irma

25, 18 and 56% in the north, south and along-track sectors, respectively, during the first post-storm week. The Irma-induced chl-a concentration increase over the entire EEZ of Cuba was comparable with climatological records (Mann-Whitney test, $p > 0.05$) during the first two post-storm weeks, while the increase along track was significantly higher (Mann-Whitney test, $p < 0.05$) (0.053 mg m^{-3}) than climatology observed at this scale (0.016 mg m^{-3}) (Avila-Alonso et al. 2019). Overall, the most remarkable biological response to Irma was the extension of an HCP in the eastern GoM during its first post-storm week, which reached the northwestern EEZ of Cuba during some days of the first post-storm week. The chl-a concentration increase after the TCs passage has been associated with vertical transport pathways driving the enhancement of nutrient concentration in the upper ocean and/or vertical transport of chl-a from greater depths. However, the increased oceanic biological response after the passage of a TC can also be driven by horizontal transport of chl-a rich waters from coastal areas adjacent to the TC trajectory (Avila-Alonso et al. 2019), as well as from remote regions of the GoM as will be shown in this study.

During Irma's pre-storm week, the chl-a concentration in the northeastern GoM was high and a HCP extended along the northeastern front of the Loop Current up to approximately 26°N latitude (i.e. I in Fig. 4a). At this time, chl-a-rich waters of 0.14 mg m^{-3} entered the northwestern sector of the EEZ of Cuba following the Loop Current circulation. In general, these chl-a enriched waters flowed at a distance of 50 km from the northwestern coast of Cuba. In contrast, during the first post-storm week the HCP extended in a more southern direction up to approximately 24°N latitude (i.e. I in Fig. 4b). However, at some days, the distance between the northwestern coast of Cuba and the waters of the HCP (with chl-a concentration of 0.2 mg m^{-3}) was only 12 km (Fig. 4c). Moreover, a moderate entrainment of chl-a-rich waters to the interior GoM from the west side of the Mississippi River delta was observed during the first post-storm week (i.e. II in Fig. 4b), which was more pronounced than in the pre-storm week (i.e. II in Fig. 4a).

3.3 Oceanic response in the eastern Gulf of Mexico

3.3.1 Origin of the high chlorophyll plume

Irma induced an increased chl-a concentration in the northeastern GoM and the suitable oceanographic conditions to enhance the offshore transport of these chl-a-rich waters. In this section, we analyse the mechanisms induced by Irma that led to this chl-a increase and we verify the riverine/coastal origin of the HCP. In general, Irma led to a mean chl-a anomaly of 0.084 mg m^{-3} during its first post-storm week in the area delineated by the rectangle in Fig. 2b. This increased chl-a concentration appears to have been driven by both vertical and horizontal transport pathways. The surface waters in the rectangular area in Fig. 2b cooled, on average, − 1.24 °C during the first post-storm week with the strongest cooling of − 1.8 °C at day + 7 (Fig. 5a). This cooling was partially driven by vertical mixing, since the MLD showed a considerable deepening during and immediately after the passage of Irma (Fig. 5b). Because the tongue of cool waters extended mainly over the West Florida Shelf, data derived from SMARTS climatology (i.e. D20 and OHC) showed a limited spatial coverage in this area, so, we did not analyse those variables in a spatially averaged way. Nevertheless, in Fig. 5c and d we observe that the D20 values were lower during the first post-storm week as compared with the pre-storm week in an area close to the tongue of cool waters, which indicates that upwelling could also have influenced the SST decrease in some areas of the northeastern GoM and consequently the biological response.

On the other hand, Irma led to heavy rainfall along its trajectory. Although the largest accumulated rainfall estimates on the basis of the NASA Integrated Multi-satellite Retrievals for Global Precipitation Measurement constellation were higher than 20 in. (512 mm) over Cuba (https://disasters.nasa.gov/hurricane-irma-2017), rainfall also affected the west coast of Florida. This explains the increased river discharge in several stations of the United States Geological Survey Water Resources Program (https://waterwatch.usgs.gov) along the west coast of Florida after the passage of Irma (Fig. 6). We found that as the water discharge increased, its temperature decreased (see station FL_02359170 in Fig. 6), which could also have contributed to the post-storm cooling in coastal areas. Moreover, a sudden and extensive SST drop after the passage of a hurricane near coastal areas can be influenced by offshore advection of cooler shelf/slope waters by the storm (Oey et al. 2006). Accordingly, this could explain in part the extensive SST cooling in the northeastern GoM during the first post-storm week of Irma (Fig. 2b). Moreover, hurricanes can change the biogeochemistry and productivity of coastal regions due to their impact on river discharge and land runoff (Gilbes et al. 2001). Thus, phytoplankton production in the northeastern GoM could have also been fuelled after the passage of Irma given the consequent nutrient deposition by rivers (Anglès et al. 2015).

The low chl-a concentration at the west side of the HCP (Fig. 4a, b) suggests that it could have originated from horizontal advection of riverine/coastal waters from the northeastern GoM that entrained the Loop Current circulation. da Silva and Castelao (2018) observed river plumes in the GoM

Fig. 5 Daily mean evolution of anomalies of (**a**) sea surface temperature (SST) and (**b**) mixed layer depth (MLD) in the area delineated by the rectangle in (**c**) in the eastern Gulf of Mexico before and after the passage of Irma. The grey bands indicate the forced stage of Irma in this area. Weekly mean 20 °C isotherm depth (D20) in the (**c**) pre- and (**d**) first post-storm week of Irma. The arrow in (**d**) indicates an area where D20 shoaled after the passage of Irma. The white pixels indicate no data

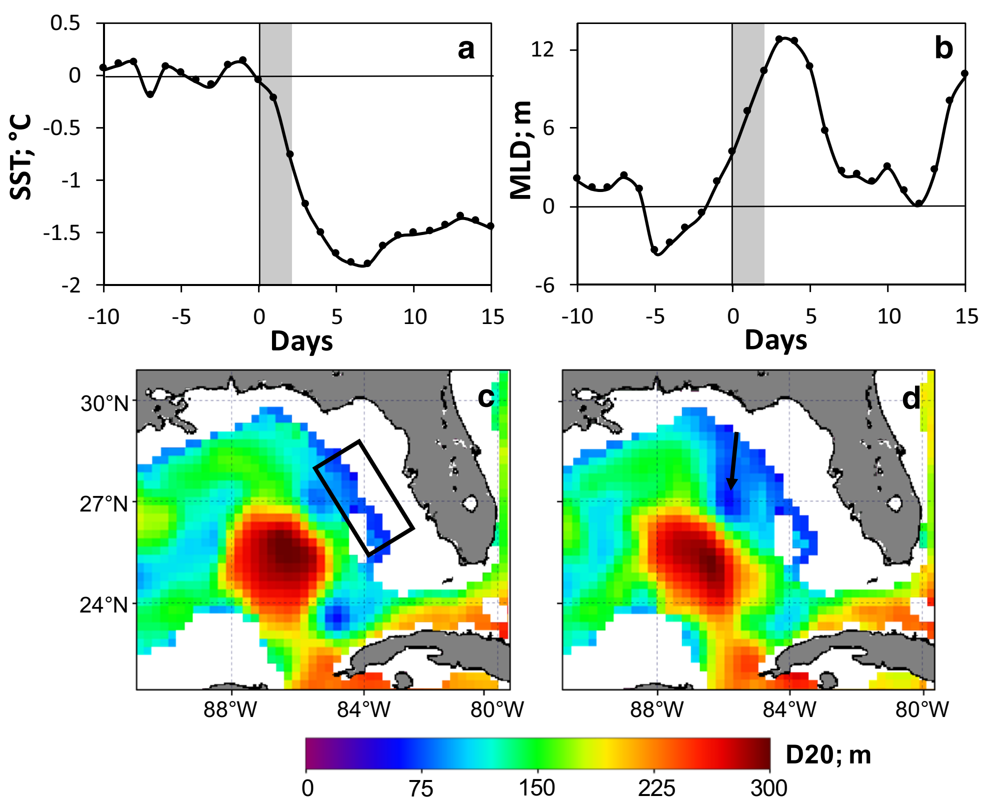

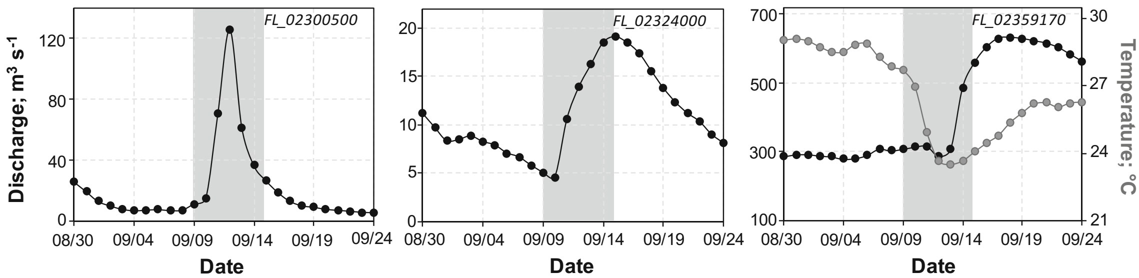

Fig. 6 River discharge and water temperature in stations along the west coast of Florida (FL) during the pre- and two post-storm weeks of Irma. The station number according to the United States Geological Survey is indicated in the upper right corner (i.e. from east to west in Fig. 2b, FL_02300500 Little Manatee River near Wimauma (27°40′15″ N, 82°21′ 10″ W), FL_02324000 Steinhatchee River near Cross City (29°47′ 11″ N, 83°19′ 18″ W) and FL_02359170 Apalachicola River near Sumatra (29°56′ 57″, 85°00′ 56″)). The grey bands indicate the first post-storm week of Irma

as waters with a high content of terrigenous DOC that were transported along the boundary of a Loop Current eddy; hence, an isolated pool of oceanic waters with low terrigenous DOC content in the eddy interior was observed. Figure 7a shows the mean values of CDM in the eastern GoM during the first post-storm week of Irma, which indicate a similar spatial pattern as the HCP, and thereby confirms the riverine origin of these waters. On the other hand, although a_{ph} was also elevated in the West Florida Shelf and the northeastern GoM, it showed lower values than CDM (Fig. 7), which agrees with the findings of Acker et al. (2009). The low values of a_{ph} can be related with the decay of phytoplankton along the path of the plume (Hu et al. 2005).

For what concerns SSS, we observed a clear progressive expansion of low-salinity waters from the northeastern GoM to the central basin and the northwestern waters of the EEZ of Cuba during the first post-storm week of Irma (Fig. 8). In general, low-salinity waters are transported first eastward along the northern GoM continental shelf, then southwestward along the edge of the West Florida Shelf, before reaching the deep GoM and the Florida Strait (Fig. 8), which corroborates the findings of Le Hénaff and Kourafalou (2016). Besides, during the first post-storm week of Irma, low-salinity waters emerged from the southwestern coast of the Florida Peninsula and joined the low-salinity filament coming from the northern GoM (Fig. 8). On the other hand, during the pre-storm week of Irma, the spatial distribution of low-salinity waters was similar to that observed on 9 September (Fig. 8), which in turn agrees with the typical spatial pattern in August (Morey et al. 2003b).

3.3.2 Drivers of the high chlorophyll plume

During the pre-storm week of Irma, southwesterly winds affected the northeastern GoM, while northeasterly winds prevailed during the first post-storm week (Fig. 9a, b). Besides, during these weeks an anticyclonic eddy at the upper front of the Loop Current impacted the northern GoM offshore circulation beyond 28°N (Fig. 9c, d). During the first post-storm week, the east side currents of this eddy intensified up to a mean speed of 0.26 m s^{-1}, whereas this was 0.14 m s^{-1} during the pre-storm week (Fig. 9c, d). On the other hand, during the first post-storm week of Irma a cyclonic eddy formed in the Apalachee Bay (Fig. 9d), leading to the formation of an anticyclonic-cyclonic eddy pair. The formation of the cyclonic or cold-core eddy could have been associated

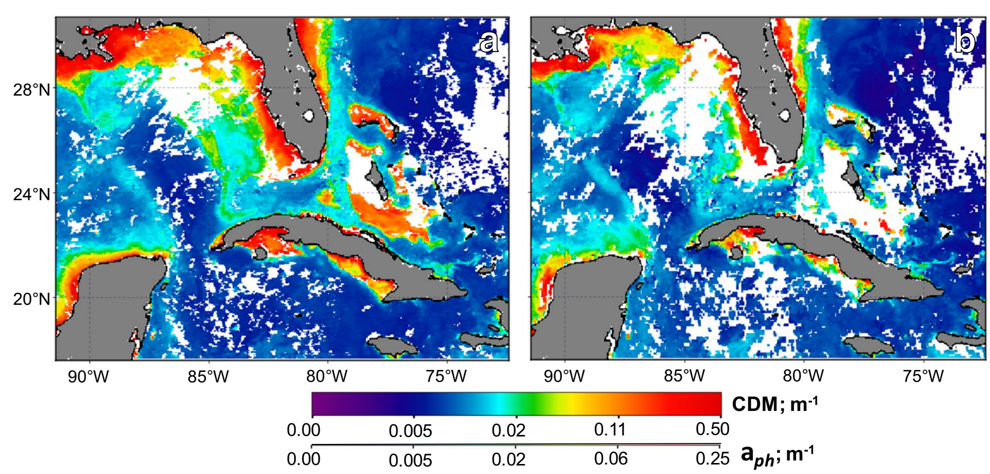

Fig. 7 Weekly mean (**a**) coloured dissolved and detrital organic material absorption coefficient at 443 nm (CDM) and (**b**) phytoplankton absorption coefficient at 443 nm (a_{ph}) in the first post-storm week of Irma. The white pixels are due to clouds

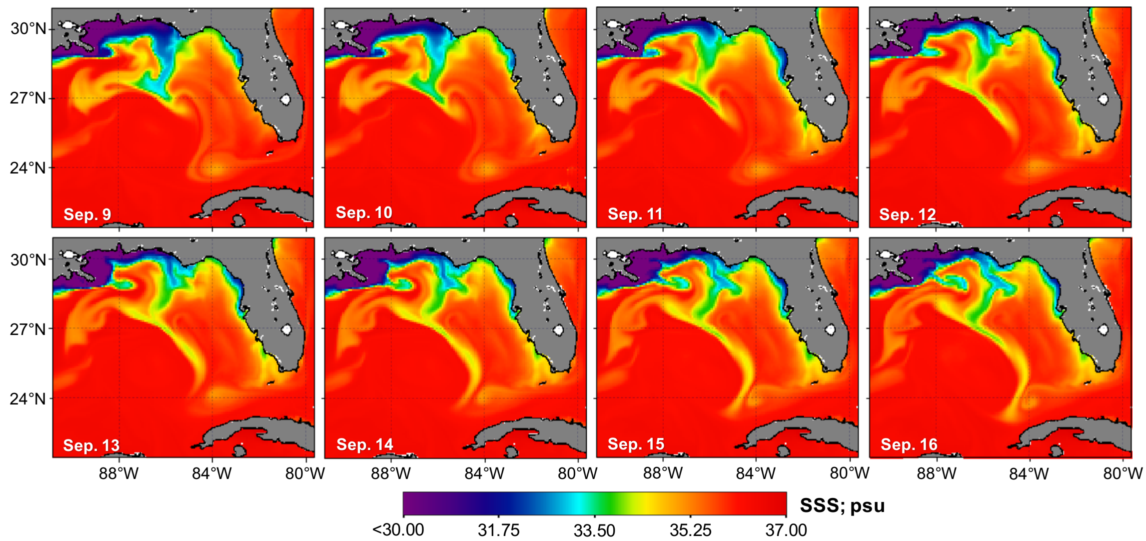

Fig. 8 Daily evolution of the sea surface salinity (SSS) in the first post-storm week of Irma

with the cooling following the passage of Irma in this region (Fig. 2b) since the post-storm SST decrease has been related with oceanic cyclonic rotation (Walker et al. 2005a; Gierach and Subrahmanyam 2008). Overall, TCs can intensify pre-existing cyclonic eddies and generate new ones as well (Sun et al. 2014). Hence, it has been suggested that wind forcing of TCs could be one of the genesis mechanisms of cold-core eddies (Sun et al. 2010).

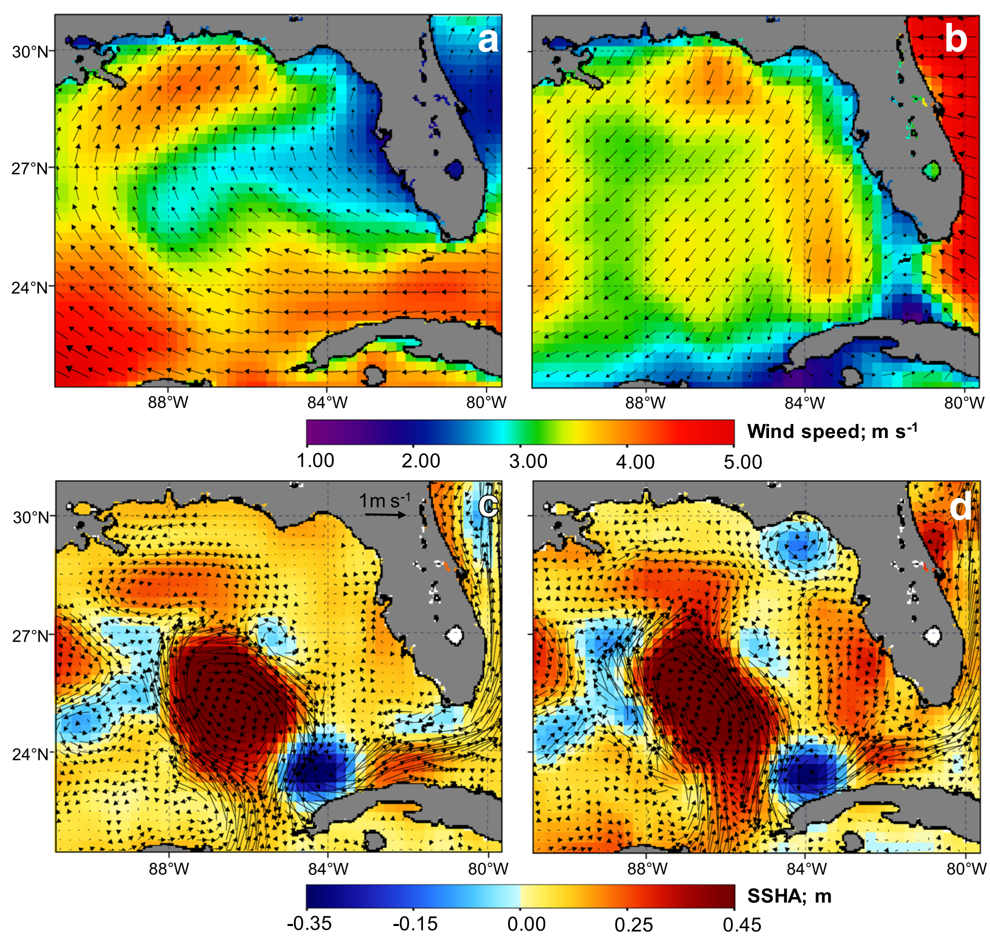

Fig. 9 Weekly mean (**a**, **b**) wind speed and (**c**, **d**) sea surface height anomaly (SSHA) with wind and geostrophic current vectors superimposed, respectively, in the pre- (left panel) and first post-storm (right panel) weeks of Irma

4 Discussion

4.1 Sea surface temperature response

The weak SST cooling in the waters of the EEZ of Cuba following the passage of Irma might be related to (1) the fact that the EEZ was impacted by the left-side quadrants of this hurricane and (2) the thermal structure of the waters surrounding Cuba. It has been reported that the oceanic responses such as upwelling, cooling and deepening of the isothermal layer are more evident on the right side of TCs (Price 1981; Shay et al. 1992; Hanshaw et al. 2008; Gierach and Subrahmanyam 2008; Fu et al. 2014). This bias is more obvious during strong and fast moving TCs (Stramma et al. 1986; Fu et al. 2014), which largely agrees with the general traits of Irma (see Sect. 3.1). Indeed, according to the TC report of the NHC, most of the deep convection of Irma was located well to the northeast of its centre (i.e. right-front quadrant) while it moved across northern Florida, and the strongest winds were confined to the northeast coast of Florida and southeastern Georgia (see Fig. 8b in the Irma TC Report).

However, wind intensity and propagation speed—which govern the rightward bias—cannot be the sole drivers of the reduced cooling (Chiang et al. 2011). The latter also indicates oceanic conditions that are relatively insensitive to atmospheric perturbations (e.g. weak ocean stratification and deep mixed layers) (Lloyd and Vecchi 2011). In general, the SST response is largest where cold waters are near the sea surface, i.e. where the mixed layer is thin and the upper thermocline is shallow (Price 1981; Chiang et al. 2011). Thus, the magnitude of the SST cooling due to mixing and entrainment is partly tied to the thermal structure of the ocean lying beneath the TC (Meyers et al. 2016). Subtropical waters like the ones of the Caribbean Sea are warm up to great depths, which increases their OHC (Shay et al. 2000). We found that during the pre-storm week of Irma, mean D20 values in the northern, southern and along-track sectors of the EEZ of Cuba were 196, 233 and 221 m, respectively, which indicates that the water column was warm up to great depths.

The more intense physical response in the northern sector of the EEZ as compared with that in the southern sector was largely caused by their different oceanographic conditions. Although the centre of Irma crossed the northern waters of Cuba, in general, wind speed anomalies were similar in both sectors (Fig. 3a) due to the large extent of the strong winds of Irma. Yet, the mixed layer depening was more pronounced in the northern waters than in the southern ones (Fig. 3b). It has been reported that the southern waters of Cuba show a higher resistance to TC-induced cooling than the northern ones (see Fig. 5b in Vincent et al. 2012) as a consequence of their deeper MLDs as compared with the northern waters. In general, a deep mixed layer has been associated to a weak SST cooling (Shay et al. 2000). Considering the classification criterion of Wang et al. (2016), i.e. shallow mixed layer (< 30 m) and deep mixed layer (> 30 m), we found that 44 and 67% of the pixels within the northern and southern sectors of the EEZ, respectively, had deep mixed layers during the pre-storm week of Irma.

The temporal variability of the MLD in the EEZ is rather consistent with reports in other regions of the world (e.g. Foltz et al. 2015; Prakash et al. 2018). In general, during and immediately following the cyclone's passage, the MLD can deepen sharply by wind-driven mixing and entrainment (Girishkumar et al. 2014; Foltz et al. 2015; Zhang et al. 2016; Prakash et al. 2018), but then, this process is countered by strong upwelling events at the beginning of the relaxation stage, which lead to a shoaling of the thermocline and MLD (Prakash et al. 2018). After that, the MLD oscillates (shoaling/deepening) while its mean depth can remain more or less the same (Girishkumar et al. 2014; Foltz et al. 2015; Zhang et al. 2016; Prakash et al. 2018).

4.2 Chlorophyll-a response

The positive chl-a concentration anomalies during the first and the second post-storm weeks in the EEZ of Cuba (Fig. 4d) agree with previous studies reporting blooms lasting about 2–3 weeks after a TC passage (Babin et al. 2004; Hanshaw et al. 2008; Avila-Alonso et al. 2019). The highest values of the post-storm chl-a anomalies along the hurricane track are consistent with the most negative SST anomalies at this scale (Figs. 2c and 4d). Thus, the vertical processes driving the SST decrease also influence the chl-a response. Mixing and upwelling can lead to vertical transport of nutrient and/or chl-a from the nitracline and/or the deep chlorophyll maximum, respectively, fuelling phytoplankton production and enhancing, in general, the surface chl-a concentration. However, given the close proximity of coastal waters to the deep oceanic ones along Irma's track, horizontal transport of chl-a-rich waters could also have influenced the biological post-storm response at this scale. This also holds for the northern sector of the EEZ since, for instance, after the passage of Irma, a chl-a filament of approximately 155 km length extended from the northeastern coast of Cuba to the adjacent oceanic waters from 14 to 19 September (Fig. 4c). On the other hand, as we have indicated before, coastal productive waters advected horizontally from remote regions of the GoM also influenced the post-storm chl-a concentration in the northwestern waters of Cuba (Fig. 4b, c).

The high chl-a concentration in the northeastern GoM and the offshore extension of the HCP during the pre- and post-storm weeks of Irma (Fig. 4a, b) agree with their seasonal variability in the region (Martínez-López and Zavala-Hidalgo 2009; Son et al. 2012; Muller-Karger et al. 2015; da Silva and Castelao 2018). Despite this natural variability, the high chl-a values during the pre-storm week might have been influenced by Hurricane Harvey, which affected the northwestern GoM during the week before the pre-storm week of Irma. Several studies have reported high rainfall amounts associated with Harvey in the western GoM (e.g. Risser and Wehner 2017; Trenberth et al. 2018), extending over the entire northern coast of the GoM (see Fig. 8 in the Harvey TC Report and Fig. 5 in Trenberth et al. 2018). This rainfall appears to have increased discharge in stations along the coast of Alabama and Mississippi at the beginning of the pre-storm week of Irma (Fig. 10), which in turn, could have stimulated phytoplankton production at this time.

4.2.1 High chlorophyll-a plume

For what concerns the mechanisms driving the HCP variability in the eastern GoM, the cyclonic circulation of Harvey may have influenced the strong southwesterly winds observed in the northeastern GoM during the pre-storm week of Irma (Fig. 9a). It has been reported that the east- and southeastward advection of riverine plumes in the GoM can result from the forcing of south- and southwesterly winds, which are common in spring and summer over the northern GoM (Morey et al. 2003a; Walker et al. 2005b; Schiller et al. 2011; Jones and Wiggert 2015; Le Hénaff and Kourafalou 2016). Since wind-induced plumes occur in short time frames of 3–7 days (da Silva and Castelao 2018), southwesterly winds could have led to an eastward movement of the Mississippi River waters during the pre-storm week of Irma, probably reinforced by the anticyclonic circulation at the upper front of the Loop Current at this time (Fig. 9c). This anticyclonic circulation could have contributed to the subsequent cross-shelf entrainment of the chl-a-rich waters to the interior GoM.

The extension of the HCP during the first post-storm week of Irma (Fig. 4b, c) appears to be related to its passage across the Florida Peninsula. Irma not only led to an increased chl-a concentration in the northeastern GoM, but it also reinforced the oceanic mechanisms to extend the HCP to the interior GoM. During the first post-storm week of Irma, northeasterly winds dominated the wind regime in the eastern GoM, which was influenced by the cyclonic circulation of this major hurricane (Fig. 9b). Northeasterly winds drive westward flows of the Mississippi River waters to the Louisiana-Texas Shelf (Walker et al. 2005b; Schiller et al. 2011), which could have enhanced the entrainment of chl-a-rich waters to the interior GoM from the west of the Mississippi River Delta (i.e. II in Fig. 4b). However, northeasterly winds can also lead to the advection of coastal waters to the interior GoM, as was observed after the passage of Hurricane Katrina (2005) near Florida Peninsula (Acker et al. 2009). This might explain the filament of low-salinity waters extending from the southwestern coast of the Florida Peninsula and joining the main low-salinity filament coming from the northern GoM (Fig. 8). Besides, wind-driven advection of coastal waters could also have contributed to the high chl-a concentration, CDM and a_{ph} over the West Florida Shelf at this time (Figs. 4b and 7). Storms passing over the ocean can affect the flow of marine currents (Oey et al. 2006; Ezer et al. 2017; Ezer 2018). Moreover, Irma affected the northeastern GoM with intense winds blowing southward on some days (e.g. on September 11) in this area. Hence, the anti-clockwise winds of Irma could have stimulated an increased cross-shelf flow of waters to the interior GoM.

Furthermore, the extension of the HCP in the eastern GoM during the first post-storm week of Irma (Fig. 4b) appears to be related with the interaction of riverine/coastal waters with the energetic eddy field near the shelf break of the northern GoM (Morey et al. 2003a; Morey et al. 2003b). Overall, even if the wind regime becomes irregular and unfavourable for the offshore transport of Mississippi River waters, mesoscale circulation can transport these waters to the central GoM (Schiller et al. 2011). The Loop Current system is a major factor in the offshore spreading of waters from the Mississippi River Delta to the GoM Basin interior (Androulidakis and Kourafalou 2013), connecting the coastal and oligotrophic waters in the GoM (Schiller et al. 2011). In particular, interactions with the Loop Current and associated eddies play a critical role transporting the Mississippi-Atchafalaya River System plumes offshore on short time scales (i.e. days to weeks) (da Silva and Castelao 2018).

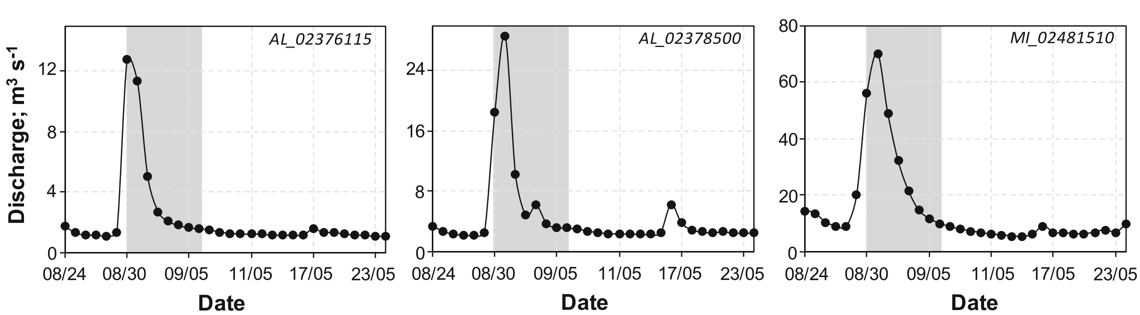

Fig. 10 River discharge in stations along the coast of Alabama (AL) and Mississippi (MI). The station number according to the United States Geological Survey is indicated in the upper right corner (i.e. from east to west in Fig. 2b, AL_02376115 Fish River near Silver Hill (30°29′ 53′ N, 87°20′ 09″ W), AL_02378500 Elevenmile Creek near Pensacola (30°32′ 43″N, 87°47′55″W) and MI_02481510 Wolf River near Landon (29°56′ 57″ N, 85°00′ 56″W)). The grey bands indicate the pre-storm week of Irma

The offshore transport of these waters takes place when the Loop Current system is well extended and close to the shelf break of the northern GoM (Hu et al. 2005; Schiller et al. 2011), as was observed during the pre- and post-storm weeks of Irma (Fig. 9c, d). In addition, the intensification of geostrophic currents during the first post-storm week, together with the formation of an eddy pair near the shelf break (Fig. 9d), could have favoured the cross-shelf advection of chl-a-rich waters into the central GoM in agreement with previous reports (Chassignet et al. 2005; Jones and Wiggert 2015; da Silva and Castelao 2018). Thus, both winds and marine currents stimulated the transport of chl-a coastal-rich waters to the interior GoM during the first post-storm week of Irma.

The extension of the HCP during Irma first post-storm week could have important ecological implications, as it connected the waters of the northern GoM and northwestern Cuba. This long distance transport of coastal and riverine waters is important for the dispersal of valuable fishing resources since a high density of larval and juvenile fishes in waters of the Mississippi River plumes have been reported (Govoni et al. 1989; Grimes and Finucane 1991). Furthermore, it has been suggested that the reduced salinity and nutrient enriched waters of the Mississippi River plume could enhance the microbial diversity in marine environments of the northern GoM as the plume migrates away from the river mouth and mixes with seawater (Mason et al. 2016).

5 Conclusions

Hurricane Irma induced a weak mean SST cooling in the waters of the Cuban EEZ during its first two post-storm weeks because the EEZ was mainly impacted by the left-side quadrants of this hurricane and the thermal structure of the waters surrounding Cuba. A considerable subsurface cooling only occurred in the waters along its trajectory, which were exposed to the most intense winds, and consequently to the highest deepening of the MLD and extensive upwelling. However, despite this limited oceanic cooling, the chl-a concentration response was comparable with climatological records over the entire EEZ. Hence, we conclude that horizontal advection of coastal waters and entrainment of chl-a-rich waters from remote regions of the GoM to the oceanic waters of the Cuban EEZ contributed to the observed post-storm biological response. For what concerns the northeastern GoM, a considerable increase in the chl-a concentration occurred after the passage of Irma, driven by both vertical and horizontal transport pathways. Moreover, an HCP of riverine/coastal origin extending from the northern GoM to the interior GoM was observed during the pre- and the post-storm weeks of the Irma. During the first post-storm week of Irma, this HCP extended southward and chl-a-rich waters flowed near the northwest coast of Cuba following the Loop Current circulation. This extension was driven by winds, by the intensification of the geostrophic currents in an anticyclonic eddy at the upper front of the Loop Current and by the formation of an anticyclonic-cyclonic eddy pair in the northeastern GoM during the first post-storm week of Irma.

Acknowledgements We thank the Upper Ocean Dynamics Laboratory at the University of Miami Rosenstiel School of Marine and Atmospheric Sciences for kindly providing us the computed ocean mixed layer depth data.

Funding information This work was supported by the Special Research Fund (BOF) of Ghent University, Belgium, Grant Code 01W03715. For satellite products presented in this work, please contact the corresponding author at davila@uclv.cu.

References

Acker J, Lyon P, Hoge F, Shen S, Roffer M, Gawlikowski G (2009) Interaction of Hurricane Katrina with optically complex water in the Gulf of Mexico: interpretation using satellite-derived inherent optical properties and chlorophyll concentration. IEEE Geosci Remote Sens Lett 6(2):209–213

Androulidakis YS, Kourafalou VH (2013) On the processes that influence the transport and fate of Mississippi waters under flooding outflow conditions. Ocean Dyn 63:143–164

Anglès S, Jordi A, Campbell L (2015) Responses of the coastal phytoplankton community to tropical cyclones revealed by high-frequency imaging flow cytometry. Limnol Oceanogr 60(5): 1562–1576

Atlas R, Hoffman RN, Ardizzone J, Leidner SM, Jusem JC, Smith DK, Gombos D (2011) A cross-calibrated, multiplatform ocean surface wind velocity product for meteorological and oceanographic applications. Bull Am Meteorol Soc 92(2):157–174

Avila-Alonso D, Baetens JM, Cardenas R, De Baets B (2019) The impact of hurricanes on the oceanographic conditions in the Exclusive Economic Zone of Cuba. Remote Sens Environ 233:111339. https://doi.org/10.1016/j.rse.2019.111339

Babin SM, Carton JA, Dickey TD, Wiggert JD (2004) Satellite evidence of hurricane-induced phytoplankton blooms in an oceanic desert. J Geophys Res Oceans 109(C03043). https://doi.org/10.1029/2003JC001938

Bender MA, Ginis I, Kurihara Y (1993) Numerical simulations of tropical cyclone-ocean interaction with a high-resolution coupled model. J Geophys Res Atmos 98(D12):23245–23263

Boss E, Zaneveld JRV (2003) The effect of bottom substrate on inherent optical properties: evidence of biogeochemical processes. Limnol Oceanogr 48(1, part2):346–354

Briones-Fourzán P, Candela J, Lozano-Álvarez E (2008) Postlarval settlement of the spiny lobster *Panulirus argus* along the Caribbean coast of Mexico: patterns, influence of physical factors, and possible sources of origin. Limnol Oceanogr 53(3):970–985

Cerdeira-Estrada S, Muller-Karger F, Gallegos-Garcia A (2005) Variability of the sea surface temperatures around Cuba. Gulf Mexico Sci 23(2):161–171

Chassignet E, Hurlburt O HEand Smedstad, Barron C, Ko D, Rhodes R, et al (2005) Assessment of data assimilative ocean models in the Gulf of Mexico using ocean color. In: Sturges W, Lugo-Fernandez A (eds) Circulation in the Gulf of Mexico: Observations and Models :87–100

Chiang TL, Wu CR, Oey LY (2011) Typhoon Kai-Tak: an ocean's perfect storm. J Phys Oceanogr 41(1):221–233

D'Asaro EA, Sanford TB, Niiler PP, Terrill EJ (2007) Cold wake of Hurricane Frances. Geophys Res Lett 34:(L15609). https://doi.org/10.1029/2007GL030160
da Silva CE, Castelao RM (2018) Mississippi River plume variability in the Gulf of Mexico from SMAP and MODIS-Aqua observations. J Geophys Res Oceans 123(9):6620–6638
Dierssen HM, Zimmerman RC, Drake LA, Burdige D (2010) Benthic ecology from space: optics and net primary production in seagrass and benthic algae across the Great Bahama Bank. Mar Ecol Prog Ser 411:1–15
Domingues R, Goni G, Bringas F, Lee SK, Kim HS, Halliwell G, Dong J, Morell J, Pomales L (2015) Upper ocean response to Hurricane Gonzalo (2014): salinity effects revealed by targeted and sustained underwater glider observations. Geophys Res Lett 42(17):7131–7138
Donlon CJ, Martin M, Stark J, Roberts-Jones J, Fiedler E, Wimmer W (2012) The Operational Sea Surface Temperature and Sea Ice Analysis (OSTIA) system. Remote Sens Environ 116:140–158
Ezer T (2018) On the interaction between a hurricane, the Gulf Stream and coastal sea level. Ocean Dyn 68(10):1259–1272
Ezer T, Atkinson LP, Tuleya R (2017) Observations and operational model simulations reveal the impact of Hurricane Matthew (2016) on the Gulf Stream and coastal sea level. Dyn Atmos Oceans 80: 124–138
Farfán LM, D'Sa EJ, Kb L, Rivera-Monroy VH (2014) Tropical cyclone impacts on coastal regions: the case of the Yucatán and the Baja California Peninsulas, Mexico. Estuar Coasts 37(6):1388–1402
Fischer G, Karakaş G (2009) Sinking rates and ballast composition of particles in the Atlantic Ocean: implications for the organic carbon fluxes to the deep ocean. Biogeosciences 6(1):85–102
Foltz GR, Balaguru K, Leung LR (2015) A reassessment of the integrated impact of tropical cyclones on surface chlorophyll in the western subtropical North Atlantic. Geophys Res Lett 42(4):1158–1164
Fu H, Wang X, Chu PC, Zhang X, Han G, Li W (2014) Tropical cyclone footprint in the ocean mixed layer observed by Argo in the Northwest Pacific. J Geophys Res Oceans 119(11):8078–8092
Fuentes Yaco C, Holguín EV, Devred T, Platt T, Sathyendranath S, Halfar J, Orta LG, Borges J (2007) Teledetección del impacto del Huracán Ignacio (2003) en el Pacífico tropical oriental. In: Hernández de la Torre B, Gaxiola Castro G (eds) Carbono en ecosistemas acuáticos de México. SEMARNAT, INE, CICESE, México, pp 279–292
Gierach MM, Subrahmanyam B (2008) Biophysical responses of the upper ocean to major Gulf of Mexico hurricanes in 2005. J Geophys Res Oceans 113(C04029). https://doi.org/10.1029/2007JC004419
Gilbes F, Armstrong RA (2004) Phytoplankton dynamics in the eastern Caribbean Sea as detected with space remote sensing. Int J Remote Sens 25(7–8):1449–1453
Gilbes F, Armstrong RA, Webb RM, Müller-Krager FE (2001) SeaWiFS helps assess hurricane impact on phytoplankton in Caribbean Sea. EOS Trans Am Geophys Union 82(45):529–533
Girishkumar M, Suprit K, Chiranjivi J, Bhaskar TU, Ravichandran M, Shesu RV, Rao EPR (2014) Observed oceanic response to Tropical cyclone Jal from a moored buoy in the south-western Bay of Bengal. Ocean Dyn 64(3):325–335
Gohin F (2011) Annual cycles of chlorophyll-a, non-algal suspended particulate matter, and turbidity observed from space and in-situ in coastal waters. Ocean Sci 7(5):705–732
Gohin F, Druon J, Lampert L (2002) A five channel chlorophyll concentration algorithm applied to SeaWiFS data processed by SeaDAS in coastal waters. Int J Remote Sens 23(8):1639–1661
Gonella J (1971) A local study of inertial oscillations in the upper layers of the ocean. Deep-Sea Res Oceanogr Abstr 18(8): 775–788. https://doi.org/10.1016/0011-7471(71)90045-3
González NM, Müller-Karger FE, Estrada SC, Pérez de los Reyes R, Río IV, Pérez PC, Arenal IM (2000) Near-surface phytoplankton distribution in the western Intra-Americas Sea: the influence of El Niño and weather events. J Geophys Res Oceans 105(C6):14029–14043
Govoni JJ, Hoss DE, Colby DR (1989) The spatial distribution of larval fishes about the Mississippi River plume. Limnol Oceanogr 34(1): 178–187
Grimes CB, Finucane JH (1991) Spatial distribution and abundance of larval and juvenile fish, chlorophyll and macrozooplankton around the Mississippi River discharge plume, and the role of the plume in fish recruitment. Mar Ecol Prog Ser 75(2):109–119
Hanshaw MN, Lozier MS, Palter JB (2008) Integrated impact of tropical cyclones on sea surface chlorophyll in the North Atlantic. Geophys Res Lett 35(L01601). https://doi.org/10.1029/2007GL031862
Hochman HT, Müller-Karger F, Walsh JJ (1994) Interpretation of the coastal zone color scanner signature of the Orinoco River plume. J Geophys Res Oceans 99(C4):7443–7455
Hu C, Nelson JR, Johns E, Chen Z, Weisberg RH, Müller-Karger FE (2005) Mississippi River water in the Florida Strait and in the Gulf Stream off Georgia in summer 2004. Geophys Res Lett 32(L14606). https://doi.org/10.1029/2005GL022942
Jaimes B, Shay LK (2009) Mixed layer cooling in mesoscale oceanic eddies during Hurricanes Katrina and Rita. Mon Weather Rev 137(12):4188–4207
Jaimes B, Shay LK (2015) Enhanced wind-driven downwelling flow in warm oceanic eddy features during the intensification of Tropical Cyclone Isaac (2012): observations and theory. J Phys Oceanogr 45(6):1667–1689
Jones EB, Wiggert JD (2015) Characterization of a high chlorophyll plume in the northeastern Gulf of Mexico. Remote Sens Environ 159:152–166
Jullien S, Menkès CE, Marchesiello P, Jourdain NC, Lengaigne M, Koch-Larrouy A, Lefèvre J, Vincent E, Faure V (2012) Impact of tropical cyclones on the heat budget of the South Pacific Ocean. J Phys Oceanogr 42(11):1882–1906
Knapp KR, Kruk MC, Levinson DH, Diamond HJ, Neumann CJ (2010) The international best track archive for climate stewardship (IBTrACS) unifying tropical cyclone data. Bull Am Meteorol Soc 91(3):363–376
Kough AS, Paris CB, Butler MJ IV (2013) Larval connectivity and the international management of fisheries. PLoS One 8(6):e64970. https://doi.org/10.1371/journal.pone.0064970
Le Hénaff M, Kourafalou VH (2016) Mississippi waters reaching South Florida reefs under no flood conditions: synthesis of observing and modeling system findings. Ocean Dyn 66(3):435–459
Leipper DF, Volgenau D (1972) Hurricane heat potential of the Gulf of Mexico. J Phys Oceanogr 2(3):218–224
Levitus S (1982) Climatological atlas of the world ocean. NOAA Profess Pap 13:1–173
Liu SS, Sun L, Wu Q, Yang YJ (2017) The responses of cyclonic and anticyclonic eddies to typhoon forcing: the vertical temperature-salinity structure changes associated with the horizontal convergence/divergence. J Geophys Res Oceans 122(6):4974–4989
Lloyd ID, Vecchi GA (2011) Observational evidence for oceanic controls on hurricane intensity. J Clim 24(4):1138–1153
Loisel H, Vantrepotte V, Ouillon S, Ngoc DD, Herrmann M, Tran V, Mériaux X, Dessailly D, Jamet C, Duhaut T et al (2017) Assessment and analysis of the chlorophyll-a concentration variability over the Vietnamese coastal waters from the MERIS Ocean color sensor (2002–2012). Remote Sens Environ 190:217–232
Lonfat M, Marks FD Jr, Chen SS (2004) Precipitation distribution in tropical cyclones using the Tropical Rainfall Measuring Mission (TRMM) microwave imager: a global perspective. Mon Weather Rev 132(7):1645–1660
Madec G (2008) NEMO ocean engine. Note du Pôle de modélisation, Institut Pierre-Simon Laplace (IPSL), France, No 27, ISSN No 1288–1619

Mallin MA, Paerl HW, Rudek J, Bates PW (1993) Regulation of estuarine primary production by watershed rainfall and river flow. Mar Ecol Prog Ser 93:199–199

Maritorena S, d'Andon OHF, Mangin A, Siegel DA (2010) Merged satellite ocean color data products using a bio-optical model: characteristics, benefits and issues. Remote Sens Environ 114(8): 1791–1804

Martínez-López B, Zavala-Hidalgo J (2009) Seasonal and interannual variability of cross-shelf transports of chlorophyll in the Gulf of Mexico. J Mar Syst 77(1–2):1–20

Mason OU, Canter EJ, Gillies LE, Paisie TK, Roberts BJ (2016) Mississippi River plume enriches microbial diversity in the northern Gulf of Mexico. Front Microbiol 7(1048). https://doi.org/10.3389/fmicb.2016.01048

Matsuoka A, Hill V, Huot Y, Babin M, Bricaud A (2011) Seasonal variability in the light absorption properties of western Arctic waters: parameterization of the individual components of absorption for ocean color applications. J Geophys Res Oceans 116:(C02007). https://doi.org/10.1029/2009JC005594

Matsuoka A, Bricaud A, Benner R, Para J, Sempéré R, Prieur L, Bélanger S, Babin M (2012) Tracing the transport of colored dissolved organic matter in water masses of the southern Beaufort Sea: relationship with hydrographic characteristics. Biogeosciences 9:925–940

Matsuoka A, Hooker B, Bricaud A, Gentili B, Babin M (2013) Estimating absorption coefficients of colored dissolved organic matter (CDOM) using a semi-analytical algorithm for southern Beaufort Sea waters: application to deriving concentrations of dissolved organic carbon from space. Biogeosciences 10(2):917–927

Matsushita B, Yang W, Chang P, Yang F, Fukushima T (2012) A simple method for distinguishing global Case-1 and Case-2 waters using SeaWiFS measurements. ISPRS J Photogramm Remote Sens 69: 74–87

Meaden GJ, Aguilar-Manjarrez J, Corner RA, O'Hagan AM, Cardia F (2016) Marine spatial planning for enhanced fisheries and aquaculture sustainability: its application in the Near East. FAO Fisheries and Aquaculture Technical Paper No. 604, Rome, p 89

Mélin F, Vantrepotte V (2015) How optically diverse is the coastal ocean? Remote Sens Environ 160:235–251

Menkes CE, Lengaigne M, Lévy M, Éthé C, Bopp L, Aumont O, Vincent E, Vialard J, Jullien S (2016) Global impact of tropical cyclones on primary production. Glob Biogeochem Cycles 30(5):767–786

Meyers PC, Shay LK, Brewster JK (2014) Development and analysis of the systematically merged atlantic regional temperature and salinity climatology for oceanic heat content estimates. J Atmos Ocean Technol 31(1):131–149

Meyers PC, Shay LK, Brewster JK, Jaimes B (2016) Observed ocean thermal response to Hurricanes Gustav and Ike. J Geophys Res Oceans 121(1):162–179

Mitrani Arenal I (2001) Caracterización general de la capa activa oceánica en los mares cercanos a Cuba y su posible enlace con el desarrollo de los ciclones tropicales. Rev Investig Mar 22(2):81–91

Mitrani Arenal I, Rodríguez OD (2001) Estructura termosalina de la capa activa oceánica en los mares cercanos a Cuba y su influencia en la formación de los ciclones tropicales. Rev Cuba Meteorol 8(1):18–24

Morel A (1980) In-water and remote measurements of ocean color. Bound-Layer Meteorol 18(2):177–201

Morey SL, Martin PJ, O'Brien JJ, Wallcraft AA, Zavala-Hidalgo J (2003a) Export pathways for river discharged fresh water in the northern Gulf of Mexico. J Geophys Res Oceans 108(C103303). https://doi.org/10.1029/2002JC001674

Morey SL, Schroeder WW, O'Brien JJ, Zavala-Hidalgo J (2003b) The annual cycle of riverine influence in the eastern Gulf of Mexico Basin. Geophys Res Lett 30(161867). https://doi.org/10.1029/2003GL017348

Muller-Karger FE, Smith JP, Werner S, Chen R, Roffer M, Liu Y, Muhling B, Lindo-Atichati D, Lamkin J, Cerdeira-Estrada S et al (2015) Natural variability of surface oceanographic conditions in the offshore Gulf of Mexico. Prog Oceanogr 134:54–76

Oey LY, Ezer T, Wang DP, Fan SJ, Yin XQ (2006) Loop current warming by Hurricane Wilma. Geophys Res Lett 33(L08613). https://doi.org/10.1029/2006GL025873

Oey LY, Ezer T, Wang DP, Yin XQ, Fan SJ (2007) Hurricane-induced motions and interaction with ocean currents. Cont Shelf Res 27: 1249–1263

Pérez-Santos I, Schneider W, Valle-Levinson A, Garcés-Vargas J, Soto I, Montoya-Sánchez R, González NM, Müller-Karger F (2014) Chlorophyll-a patterns and mixing processes in the Yucatan Basin, Caribbean Sea. Cien Mar 40(1):11–31

Prakash KR, Nigam T, Pant V (2018) Estimation of oceanic subsurface mixing under a severe cyclonic storm using a coupled atmosphere–ocean–wave model. Ocean Sci 14(2):259–272

Prescott-Allen R (2001) The well-being of nations: a country-by-country index of quality of life and the environment. Island Press, Washington, D.C., p 342

Price JF (1981) Upper ocean response to a hurricane. J Phys Oceanogr 11(2):153–175

Price JF (1983) Internal wave wake of a moving storm. Part I. Scales, energy budget and observations. J Phys Oceanogr 13(6):949–965

Price JF (2009) Metrics of hurricane-ocean interaction: vertically-integrated or vertically-averaged ocean temperature? Ocean Sci 5(3):351–368

Risser MD, Wehner MF (2017) Attributable human-induced changes in the likelihood and magnitude of the observed extreme precipitation during Hurricane Harvey. Geophys Res Lett 44:12457–12464

Schiller R, Kourafalou V, Hogan P, Walker N (2011) The dynamics of the Mississippi River plume: impact of topography, wind and offshore forcing on the fate of plume waters. J Geophys Res Oceans 116(C06029). https://doi.org/10.1029/2010JC006883

Shay LK, Elsberry RL (1987) Near-inertial ocean current response to Hurricane Frederic. J Phys Oceanogr 17(8):1249–1269

Shay LK, Black PG, Mariano AJ, Hawkins JD, Elsberry RL (1992) Upper ocean response to Hurricane Gilbert. J Geophys Res Oceans 97(C12):20227–20248

Shay LK, Goni GJ, Black PG (2000) Effects of a warm oceanic feature on Hurricane Opal. Mon Weather Rev 128(5):1366–1383

Shi W, Wang M (2007) Observations of a Hurricane Katrina-induced phytoplankton bloom in the Gulf of Mexico. Geophys Res Lett 34(L11607). https://doi.org/10.1029/2007GL029724

Shropshire T, Li Y, He R (2016) Storm impact on sea surface temperature and chlorophyll a in the Gulf of Mexico and Sargasso Sea based on daily cloud-free satellite data reconstructions. Geophys Res Lett 43(23):12199–12207

Son S, Platt T, Fuentes-Yaco C, Bouman H, Devred E, Wu Y, Sathyendranath S (2007) Possible biogeochemical response to the passage of Hurricane Fabian observed by satellites. J Plankton Res 29(8):687–697

Son YB, Gardner WD, Richardson MJ, Ishizaka J, Ryu JH, Kim SH, Lee SH (2012) Tracing offshore low-salinity plumes in the northeastern Gulf of Mexico during the summer season by use of multispectral remote-sensing data. J Oceanogr 68(5):743–760

Spencer RG, Aiken GR, Dornblaser MM, Butler KD, Holmes RM, Fiske G, Mann PJ, Stubbins A (2013) Chromophoric dissolved organic matter export from US rivers. Geophys Res Lett 40(8):1575–1579

Stramma L, Cornillon P, Price JF (1986) Satellite observations of sea surface cooling by hurricanes. J Geophys Res Oceans 96(C4): 5031–5035

Sun L, Yang YJ, Xian T, Lu Zm FYF (2010) Strong enhancement of chlorophyll a concentration by a weak typhoon. Mar Ecol Prog Ser 404:39–50

Sun L, Yang YJ, Xian T, Wang Y, Fu YF (2012) Ocean responses to Typhoon Namtheun explored with Argo floats and multiplatform satellites. Atmosphere-Ocean 50(sup1):15–26

Sun L, Li YX, Yang YJ, Wu Q, Chen XT, Li QY, Li YB, Xian T (2014) Effects of super typhoons on cyclonic ocean eddies in the western North Pacific: a satellite data-based evaluation between 2000 and 2008. J Geophys Res Oceans 119(9):5585–5598

Trenberth KE, Cheng L, Jacobs P, Zhang Y, Fasullo J (2018) Hurricane Harvey links to ocean heat content and climate change adaptation. Earth's Future 6:730–744

Vincent EM, Lengaigne M, Vialard J, Madec G, Jourdain NC, Masson S (2012) Assessing the oceanic control on the amplitude of sea surface cooling induced by tropical cyclones. J Geophys Res Oceans 117(C05023). https://doi.org/10.1029/2011JC007705

Walker ND, Leben RR, Balasubramanian S (2005a) Hurricane-forced upwelling and chlorophyll a enhancement within cold-core cyclones in the Gulf of Mexico. Geophys Res Lett 32(L18610). https://doi.org/10.1029/2005GL023716

Walker ND, Wiseman WJ Jr, Rouse LJ Jr, Babin A (2005b) Effects of river discharge, wind stress, and slope eddies on circulation and the satellite-observed structure of the Mississippi River plume. J Coast Res 21(6):1228–1244

Wang G, Wu L, Johnson NC, Ling Z (2016) Observed three-dimensional structure of ocean cooling induced by Pacific tropical cyclones. Geophys Res Lett 43(14):7632–7638

Wei J, Liu X, Jiang G (2018) Parameterizing sea surface temperature cooling induced by tropical cyclones using a multivariate linear regression model. Acta Oceanol Sin 37(1):1–10

Wu Q, Chen D (2012) Typhoon-induced variability of the oceanic surface mixed layer observed by Argo Floats in the western north Pacific Ocean. Atmosphere-Ocean 50(sup1):4–14

Zavala-Hidalgo J, Gallegos-García A, Martínez-López B, Morey SL, Brien JJ (2006) Seasonal upwelling on the western and southern shelves of the Gulf of Mexico. Ocean Dyn 56(3–4):333–338

Zhang H, Chen D, Zhou L, Liu X, Ding T, Zhou B (2016) Upper ocean response to Typhoon Kalmaegi (2014) J Geophys Res Oceans 121(8):6520–6535

Zhang H, Liu X, Wu R, Liu F, Yu L, Shang X, Qi Y, Wang Y, Song X, Xie X et al (2019) Ocean response to successive Typhoons Sarika and Haima (2016) based on data acquired via multiple satellites and moored array. Remote Sens 11(20):2360. https://doi.org/10.3390/rs11202360

Zhu W, Yu Q, Tian YQ, Chen RF, Gardner GB (2011) Estimation of chromophoric dissolved organic matter in the Mississippi and Atchafalaya river plume regions using above-surface hyperspectral remote sensing. J Geophys Res Oceans 116(C0201). https://doi.org/10.1029/2010JC006523